INSTITUTE OF PHYSICS PUBLISHING NANOTECHNOLOGY
Nanotechnology **16** (2005) 647–654 doi:10.1088/0957-4484/16/6/005

FeCo magnetic nanoneedles obtained by Co-coating haematite

Raquel Mendoza-Reséndez[1], Raul Pozas[2], M Puerto Morales[1], Pierre Bonville[3], Manuel Ocaña[2] and Carlos J Serna[1,4]

[1] Instituto de Ciencia de Materiales de Madrid, Cantoblanco, 28049 Madrid, Spain
[2] Instituto de Ciencia de Materiales de Sevilla (CSIC-UNSE), Americo Vespucio s/n, Isla de La Cartuja, 41092 Sevilla, Spain
[3] CEA, CE Saclay, Service de Physique de l'État Condensé, 91191 Gif-sur-Yvette, France

E-mail: cjserna@icmm.csic.es

Received 25 October 2004, in final form 21 January 2005
Published 9 March 2005
Online at stacks.iop.org/Nano/16/647

Abstract
Uniform FeCo magnetic nanoneedles of ∼50 nm in width and axial ratio ∼5 have been obtained by Co-coating haematite and subsequent hydrogen reduction in two steps. By this method, FeCo needle-like nanoparticles were obtained with Co contents up to 10% evenly distributed inside the particles. Higher Co contents up to 30% were incorporated by coating the Co-doped magnetite nanoneedles. No segregation of a secondary phase was observed in any case and the morphology of the particles was preserved without adding any extra element. Structural changes during the reduction process have been followed by several techniques. Although protected by an oxide layer, the final metal nanoparticles behave as single crystals, but they are composed of sub-crystals with the same crystallographic orientation and a mean diameter that decreases as the Co content increases. We found the highest reported saturation magnetization values for samples of similar size (180 emu g^{-1}). The evolution of the coercivity with the cobalt modification could arise from the changes of the microstructure and the contributions of shape and crystalline anisotropies. Time dependence magnetization measurements showed the thermal activation to be related to the presence of crystallographic sub-units within the nanoneedles.

1. Introduction

The Co modification of Fe needle-like nanoparticles can improve their hard magnetic properties and resistance against corrosion [1, 2]. These nanoneedles find interesting applications in different areas such as catalysis, magnetic recording media and, it has been recently shown, the field of biomedicine, in particular in magnetic cell separation [3–5]. Thus, high aspect ratio magnetic nanoparticles outperform commercially available magnetic beads, the most common magnetic nanoparticles used in separations, both in purity and yield of the separated cell populations [6].

Unfortunately, the preparation of uniform magnetic particles with controllable shapes other than spherical is not possible by direct precipitation in homogeneous solutions and therefore the use of a template or the synthesis of a non-magnetic precursor is required [7]. Many advances have been made in recent years in relation to the study of FeCo nanoparticles prepared using goethite as precursor and modified with cobalt by doping or coating [8–11]. In these cases, high axial ratio FeCo based needle-like nanoparticles of around 100 nm in length were obtained. However, these particles present high porosity, rather broad particle size and shape distribution, and the precursor needs to be protected with antisintering agents in order to preserve the particle morphology during the reduction process and to be stable against oxidation.

On the other hand, only a few works have been found to be concerned with the preparation of FeCo nanoneedles starting from other oxides such as haematite [12, 13]. Moreover, when cobalt was introduced by Co-coating haematite, a segregation

[4] Address for correspondence: Sor Juana Inés de la Cruz s/n, Instituto de Ciencia de Materiales de Madrid, CSIC Cantoblanco 28049-Madrid, Spain.

of spherical particles of Co_3O_4 took place when the Co percentage was higher than 10%.

In this paper, monodisperse α-Fe_2O_3 particles with needle-like morphology were prepared by homogeneous hydrolysis in solutions of an iron salt with urea in the presence of phosphate anions [14]. The advantage of using haematite as precursor instead of goethite is the possibility of having larger particles with low porosity, while keeping a very narrow particle size and shape distribution [14, 15].

The aim of this work is to develop a method of introducing Co ions inside needle-like haematite nanoparticles by two reduction steps, in such a way that the material leads to FeCo alloy preserving the particle morphology without the use of antisintering agents [16, 17]. The mechanism of formation of the Fe–Co alloy particles was followed in detail by different techniques to optimize the preparation method and try to understand the magnetic behaviours of the final material.

2. Experimental section

2.1. Sample preparation

Needle-like haematite (α-Fe_2O_3) particles, used as precursor, were prepared by ageing 0.1 M iron (III) perchlorate solutions ($Fe(ClO_4)_3{\cdot}9H_2O$, Fluka, >98%) and sodium dihydrogen phosphate (NaH_2PO_4, Fluka, >97%) at 100 °C in the presence of urea (Merck, >99%). During ageing, the solutions were kept undisturbed in tightly capped Pyrex test tubes. The precipitates were separated from their mother solutions by centrifugation at 18 000 rpm and washed several times with double distilled water until a clear supernatant was observed. Finally, the thus prepared solids were dried at 50 °C before analyses. Haematite particles of 270 nm in length and axial ratio 5 were obtained by using a 0.05 NaH_2PO_4/Fe^{3+} molar ratio (sample H), according to [14].

2.1.1. Cobalt-coating. Cobalt-coated α-Fe_2O_3 particles were prepared by first dispersing 5×10^{-3} mol of α-Fe_2O_3 powders in 150 ml of double distilled water in an ultrasonic bath and second adding to this dispersion 50 ml of a solution containing cobalt nitrate ($Co(NO_3)_2{\cdot}6H_2O$, Merck >99%) in percentages of 10, 20 and 30 wt% of (Co)/Co + Fe. Then, the pH was adjusted to 10 with NH_4OH solution and the sample kept stirred for 1 h. The resulting precipitates were washed with double distilled water and dried at 50 °C for 12 h before reduction. Samples were named 10-CoH, 20-CoH and 30-CoH.

The reduction of the haematite particles to metal was carried out in two steps in order to achieve the formation of a homogeneous Fe–Co solid solution. Thus, in the first step, Co-coated haematite particles were heated at 200 °C in vacuum for 3 h and then reduced to a Co spinel under 1 atm of hydrogen at 360 °C for another 3 h. At this stage, only the sample containing 10% of Co shows no segregation of a different phase (sample 10-CoM). Therefore, in order to obtain higher Co contents, sample 10-CoM was coated with an additional 10 and 20% of Co following the procedure described in the previous section and subjected again to the first reduction step to form the Co spinel phase (samples 20-CoM and 30-CoM).

Finally, the Co magnetite samples were reduced to metal at 400 °C under a hydrogen flow of 40 l h^{-1} for 4 h. The collected samples were cooled down to room temperature under H_2 atmosphere. Finally, a N_2 gas wetted with ethanol was passed through the sample in order to passivate the surface slightly (samples 10-CoFe, 20-CoFe and 30-CoFe). A schematic representation of the strategy used to obtain Fe–Co particles with Co contents up to 30% is shown in figure 1. In addition, a pure iron sample (Fe) was prepared for comparison.

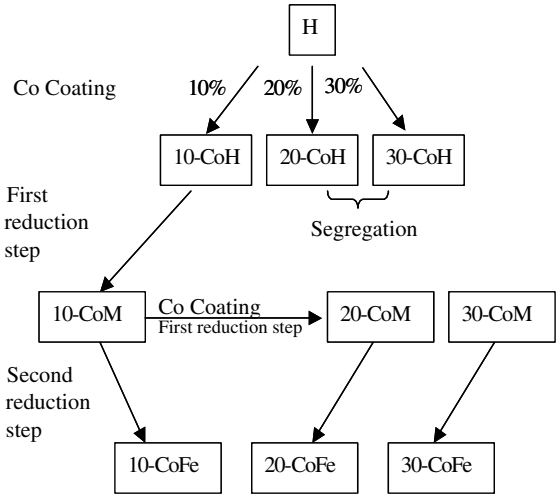

Figure 1. Schematic representation of the preparation route followed to obtain Fe–Co magnetic nanoneedle particles (CoFe) with different Co contents from haematite (H) to magnetite (M).

2.2. Characterization techniques

The phases present in the samples were identified by powder x-ray diffraction (XRD) measurements using a Philips 1710 diffractometer and Cu Kα radiation. The crystallite size of the spinel and metal particles was calculated from the full width at half maximum of the (311) and (110) reflections, respectively, using the Scherrer equation [18]. The morphology and particle size distribution were investigated using a high-resolution electron microscope (JEOL-2000 FXII). To prepare the samples for TEM observation, the powders were dispersed in toluene in an ultrasonic bath for some minutes and then a drop of this solution was deposited onto a carbon coated copper grid. In all cases, the average particle length and the standard deviation were calculated by counting around 100 particles. Fourier transform infrared spectroscopy (FTIR) spectra were measured using a Bruker IFS 66v/S spectrometer and the spectra were recorded over the frequency range from 250 to 850 cm^{-1}.

The cobalt content in the haematite samples was determined by plasma emission (ICP, Perkin-Elmer 5500). For this analysis, 100 mg of powder was first dissolved with concentrated HCl and then diluted with double distilled water. In addition, the local Co content per particle was analysed from the energy dispersive spectra (EDS) obtained using a QX2000 Link x-ray analyser installed in the electron microscope. Furthermore, surface analysis of the spinel and metal samples by x-ray photoelectron spectroscopy (XPS) was recorded in a VG Escalab 220 using the Mg Kα excitation source. Surface characterization of the haematite samples was also carried out by measuring the electrophoretic mobility of

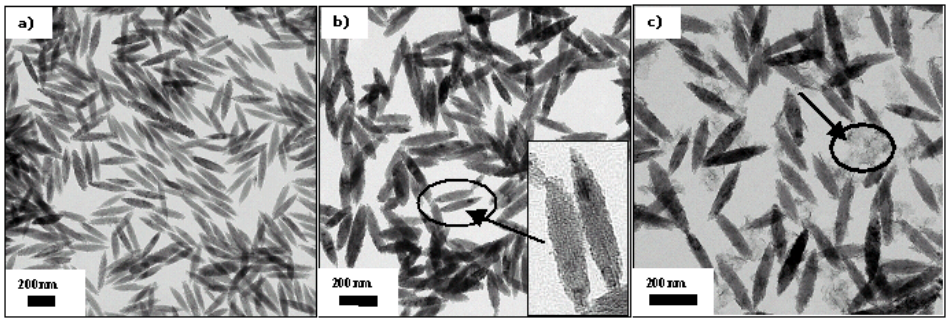

Figure 2. TEM images of pure haematite and Co-coated haematite particles: (a) sample H; (b) 10-CoH; (c) 20-CoH.

aqueous suspensions of the powders as a function of the pH using a Coulter DELSA 440. All the experiments were carried out at 25 °C, using KNO_3 as electrolyte and HNO_3 and KOH to change the pH of the suspensions.

^{57}Fe Mössbauer absorption spectroscopy was used to characterize the final metal particles. The spectra were recorded with a maximum velocity of 10 mm s^{-1} at different temperatures between 298 and 4.2 K with a ^{57}Co:Rh source. By fitting the spectra at 4.2 K, the fraction of iron oxide on the surface of the final iron particles was determined.

The magnetic characterization of the samples was carried out in a vibrating sample magnetometer (MLVSM9 MagLab 9 T, Oxford Instruments). Coercivity field (H_c) and saturation magnetization (M_s) values were obtained from the hysteresis loops recorded at room temperature with a maximum applied field of 3 T. The M_s values were evaluated by extrapolating to infinite field the experimental results obtained in the high field range where the magnetization linearly decreases with $1/H$. The activation volume V_a was obtained from the measurement of the time dependence of the magnetization around the coercive field (between 1000 and 2000 Oe). The variation of magnetization with time followed the form

$$M(t) = M(0) - S\ln(t)$$

where S is the coefficient of magnetic viscosity. Due to this linearity in $\ln(t)$, the activation volume for reversal (V_a), which describes that volume of the magnetic material which reverses coherently, can be determined following Gaunt [19].

$$V_a = k_B T/[M_s S/\chi_{irr}]$$

where $\chi_{irr}(H)$, the irreversible susceptibility, is obtained from the differential of the remanence curve and $S = -dM/d[\ln(t)]$.

3. Results and discussion

3.1. Co-coated haematite particles

Uniform haematite particles of 270 nm in length and axial ratio 5 (sample H), synthesized by precipitation with urea of iron perchlorate solution in the presence of phosphate ions ($NaH_2PO_4/Fe^{3+} = 0.05$) were used as precursor (figure 2(a)). A detailed characterization of the particles can be found elsewhere [14]. These particles were used as templates for coating with cobalt ions following the procedure described in the experimental section. It was observed that only up to 10% of Co can be deposited onto the surface of the haematite particles (figure 2(b)), while higher amounts, like 20% and 30% of Co, resulted in a different phase segregated from the haematite particles, as can be observed in figure 2(c). This is clearly illustrated by x-ray diffraction in figure 3, where the powder diffractograms of haematite and Co-coated haematite particles are compared. For sample 10-CoH the observed peaks correspond to those of pure haematite but for 20-CoH and 30-CoH new reflexions with maxima at about 19, 32, 38 and 51 of 2θ assigned to $Co(OH)_2$ were found. Ishikawa and Matijevic (1988) tried to coat haematite particles with $Co(CH_3COO)_2$ at pH 7 but a separate Co_3O_4 spinel phase was always obtained, as a result of the higher temperature (100 °C) used during the synthesis [12].

In addition, high resolution electron micrographs of sample 10-CoH show that the coating is not totally uniform (figure 2(b)) but composed by tiny particles forming a layer of around 1–2 nm thick. The presence of this amorphous $Co(OH)_2$ layer on the surface of the haematite particles was confirmed by electrophoretic measurements (figure 4). Although chemical analysis of sample 10-CoH gives a value of 8.5% Co/Fe + Co suggesting an almost complete precipitation of the initial Co added onto the haematite particles (figure 2(b)), the isoelectric point (iep) shifts to higher values after the coating (from 6.2 for sample H to 6.9 for sample 10-CoH) but always far from 11, the iep of 'pure' $Co(OH)_2$, which points to a low homogeneity of the coating.

3.2. First reduction step to magnetite

Co-coated haematite particles with about 10% of Co were then reduced at 360 °C under hydrogen atmosphere as reported in the experimental section, to promote the Co diffusion inside the particle. Under this treatment, the needle-like particle morphology is preserved (figure 5(a)). The x-ray powder diffraction pattern (figure 6) shows the formation of a cubic inverse spinel phase whose lattice parameter a of 8.39 Å is reduced from that for pure magnetite (8.42 Å), according to the incorporation of Co(II) in the octahedral positions of magnetite [20]. For samples coated with higher cobalt contents, a segregation of tiny spherical particles on the nanoneedle particle surface was clearly observed by TEM and identified as Co_3O_4 by x-ray diffraction (data not shown). The segregation of this secondary phase was previously observed by other authors, indicating that it is not possible to incorporate more than 10% Co by coating haematite [12].

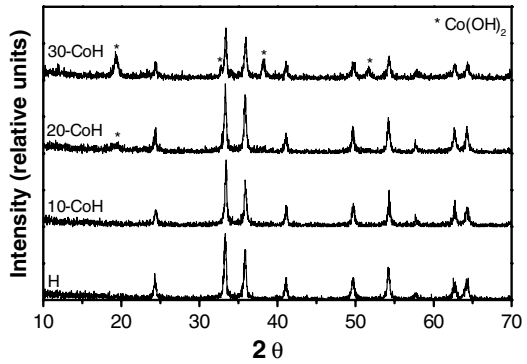

Figure 3. X-ray diffraction patterns for haematite particles coated with 10%, 20% and 30% of cobalt.

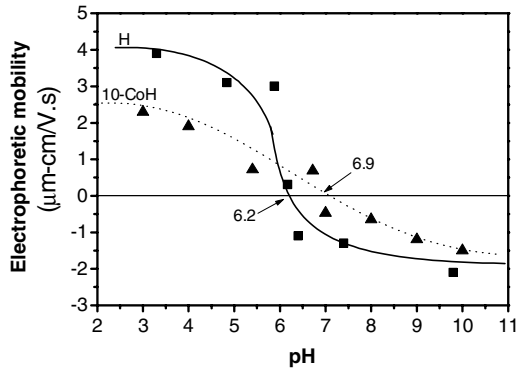

Figure 4. Electrophoretic mobility of haematite and 10% Co-coated haematite.

In order to obtain magnetite particles with Co content up to 30%, sample 10-CoM was coated with an additional 10 and 20% of Co, using the same procedure as that used with haematite and then subjected again to the first reduction step (see figure 1). In this way, single-phase magnetite particles with 18 and 27% of Co were obtained, according to the chemical analyses, without segregation of other phases as illustrated for sample 30-CoM in figure 5(b). The x-ray powder diffraction patterns also show the formation of 'pure' Co magnetites without the presence of any additional phase (figure 6). Besides, infrared spectra for CoM samples showed the two absorption bands, ν_1 and ν_2, characteristic of an inverse spinel, which shift slightly to higher wavenumbers and become more symmetric when comparing sample M and samples 10-CoM and 30-CoM (figure 7). This behaviour is in agreement with the partial substitution of Fe^{2+} by Co^{2+} in the octahedral position of Co magnetite, according to the formula $(Fe^{3+})_A(Fe^{3+}Fe^{2+}{}_{1-x}Co^{2+}{}_x)_BO_4$ [21].

XPS surface analyses were carried out to determine how Co ions extend over the particles. 13% of Co was found on the surface of the particles for sample 10-CoM, suggesting a rather homogeneous distribution of the cobalt ions inside the particle for this composition. However, the amount of Co in the surface reached a value of 54% for sample 30-CoM, indicating that the diffusion of Co ions inside the particle at this composition was very poor. Analogous results were also found for the 20% Co magnetite sample.

Therefore, the first 10% of Co introduced on the haematite surface seems to diffuse easily inside the particle during the first

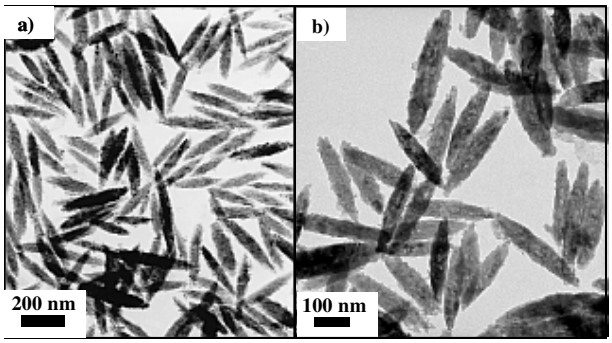

Figure 5. TEM images of magnetite particles: (a) samples 10-CoM and (b) 30-CoM.

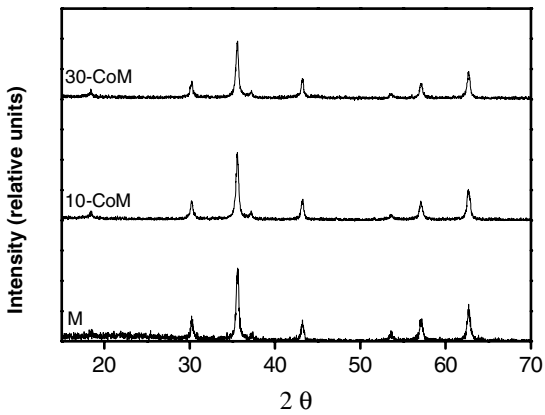

Figure 6. X-ray diffraction patterns for magnetite samples with different Co content.

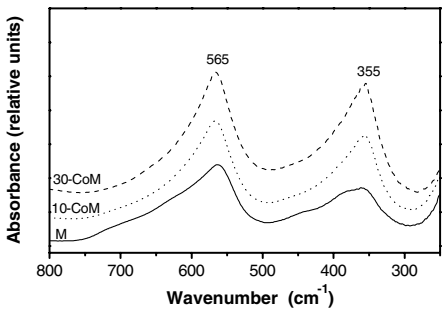

Figure 7. Infrared spectra for magnetite samples with different Co content.

reduction process, giving rise to a Co-doped magnetite which agrees well with the change in the lattice parameter of the magnetite and the XPS analysis. The formation of 10-CoM is a typical solid-state reaction between CoO (formed after heating the $Co(OH)_2$) and Fe_2O_3 to form $CoFe_2O_4$, where both thermodynamic and kinetic factors are very important [22]. After an appropriate heat treatment (360 °C in our case), the solids have partially reacted to form a layer of $CoFe_2O_4$ at the interface. The nucleation of this first layer implies that bonds must be broken and reformed and atoms must migrate. If nucleation is a difficult process, the subsequent stage involving the growth of the product layer may well be even more so. Thus, in order for the $CoFe_2O_4$ layer to grow thicker, counter-diffusion of Co^{2+} and Fe^{3+} ions must occur right through the existing $CoFe_2O_4$ product layer to the new reaction interface.

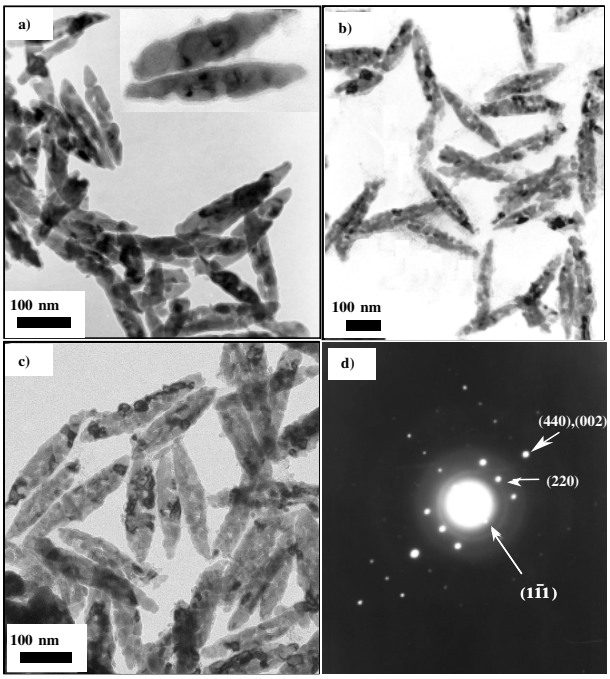

Figure 8. TEM images of metal samples with different Co contents: (a) 10-CoFe; (b) 20-CoFe; (c) 30-CoFe and (d) electron diffraction diagram obtained from one particle from sample 30-CoFe. The reflexion (002) corresponds to metallic FeCo and those of (440), (220) and (1$\bar{1}$1) reflexions to the oxide layer.

Taking into account that the diffusion rates are slow even at high temperatures, further reaction takes place only slowly and at a decreasing rate as the spinel layer grows thicker. The interdiffusion of cations through the spinel product layer is indeed the rate controlling step and that is the reason why only a certain amount, 10% of Co in this case, is incorporated to the magnetite by this method. The rest of the Co incorporated by coating the magnetite is expected to exist as a transition phase at the surface of the particles, with decreasing amount of Co towards the core [23]. It should be mentioned that Co contents up to 28% have been found incorporated into the magnetite structure when it is formed from aqueous solutions of Co and Fe salts and therefore a diffusion process is not required [24].

3.3. Second reduction step to FeCo alloy

The Co magnetite samples were reduced at 400 °C under a hydrogen flow and passivated by a nitrogen flow wetted in ethanol. Under these experimental conditions the particles maintain the needle-like morphology for all the Co contents with no segregation of secondary phases, as shown in figure 8. It should be noted that the particle morphology is preserved for all the samples although no anti-sintering elements such as aluminium or yttrium were added to protect them, as is the case when goethite is used as a precursor [4, 8, 11].

Particle size varies between 200 and 250 nm in length depending on the Co content, while the axial ratio is kept around 5. At higher resolution, transmission electron microscope images indicate that the particles are composed of several crystallites as suggested by the presence of darker zones inside each particle, leaving empty spaces between them due to the formation of pores (figures 8(a)–(c)), but

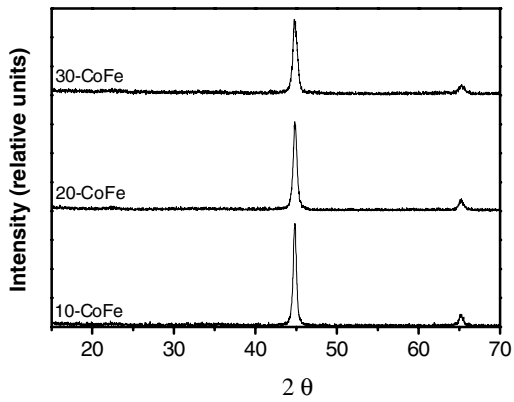

Figure 9. X-ray diffraction patterns for metal samples with different Co content.

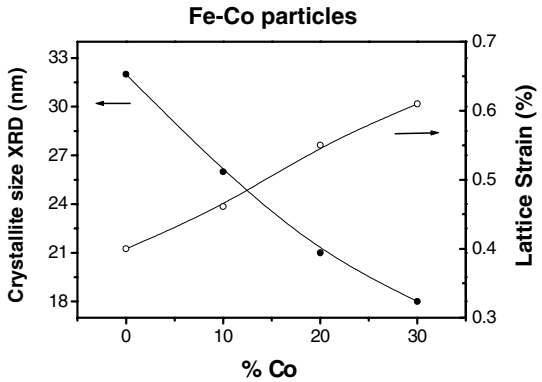

Figure 10. Crystallite size and lattice strain for metal particles as a function of the Co content.

this porosity is lower than the porosity observed in particles prepared with goethite precursors [4, 8, 9]. Furthermore, electron diffraction carried out on individual particles shows a single-crystal character with some bright spots corresponding to a body-centred-cubic lattice similar to the Fe–Co alloy, and other lighter spots corresponding to a spinel iron oxide in a close structural relationship with the first ones (figure 8(d)). Thus, the bright spot assigned to the (002) planes of the Fe–Co alloy has the same interplanar spacing as the (440) planes of the spinel, i.e. 1.48 Å. This result can only be understood if all the crystallites inside each particle have the same crystal orientation, as was previously observed in needle-like iron particles obtained from alumina-coated haematite [25]. Thus, the passivation layer (the spinel) grows with the [111] direction collinear to the [111] direction of the iron core.

For all the compositions, the XRD of the samples shows similar patterns, corresponding to a body-centred-cubic structure assigned to a Fe–Co solid solution (figure 9). However, the crystallite size decreases from 32 nm for pure iron to 18 nm for the particles with the highest cobalt content and at the same time the lattice strain increases up to 33% more than for pure metal particles (figure 10). These observations seem to be in agreement with the presence of several crystallites inside each individual particle as observed by TEM (figures 8(a)–(c)), where the number of crystallites per particle increases as the Co content increases in the sample.

Information about the homogeneity of the Co distribution in the FeCo samples as well as on the nature of the passivation

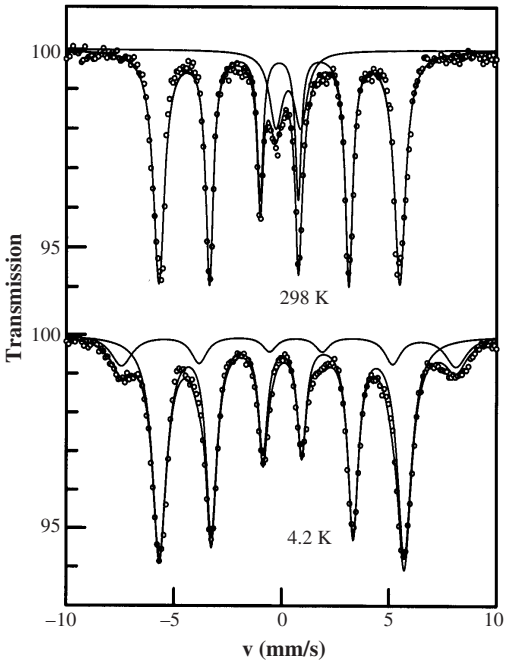

Figure 11. Mössbauer spectra at room temperature and 4.2 K for sample 10-CoFe.

layer was obtained by Mössbauer spectroscopy at 298 and 4.2 K. For all samples, the spectrum at room temperature shows two distinct components: a magnetic sextet and a non-magnetic doublet (illustrated for sample 10-CoFe in figure 11). However, at 4.2 K two different magnetic sextets were required to fit the data for all the samples (figures 11 and 12). The majority component is a magnetic sextet with parameters similar to those of α-Fe, while the minority component is a sextet with a much larger hyperfine field, characteristic of small particles of a spinel iron oxide that must be assigned to the oxide layer formed during the passivation process [17, 26]. The Co content has a small but significant effect on the hyperfine field of the first sextet, B_{hf}. Thus B_{hf} is 35.2 T for sample 10-CoFe and the spectrum has narrow lines, in agreement with the presence of about 10% of Co evenly distributed in the particles [26]. However, for the other two samples with Co contents of 20 and 30%, the lines are broader and thus a distribution of hyperfine fields is needed to fit the spectra. These distributions have maxima between 34.2 and 38 T, indicating a heterogeneous Co distribution in the particles (figure 12). It should be noted that a heterogeneous distribution of Co in the Co magnetites samples with 20 and 30% has already been observed by XPS.

Furthermore, the spectra at 4.2 K give an accurate measure of the relative proportions of iron atoms in both the iron oxide passivation layer and the metallic core by determining the relative spectral area of their sextets (figures 11 and 12). The results are included in table 1 along with an iron sample without cobalt, included for comparison. It is clear from the table that the effect of cobalt is to decrease the thickness of the surface passivation layer, reducing the oxide content in the samples from nearly 40 to around 20%, which is expected to affect its magnetic behaviour. It should be noted that the effect of cobalt on the thickness of the oxide layer is not observed when antisintering agents are added to the precursor particles [11].

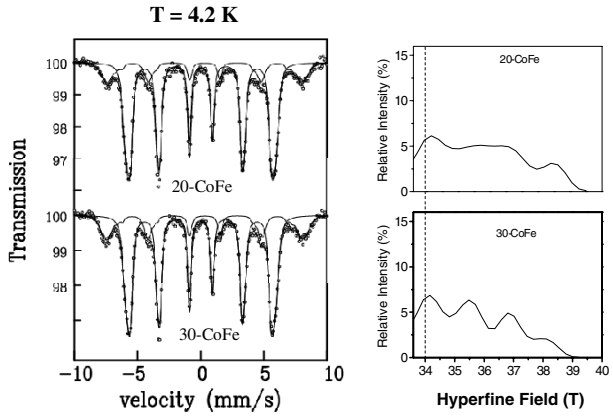

Figure 12. Mössbauer spectra at 4.2 K and hyperfine field distributions for samples 20-CoFe and 30-CoFe.

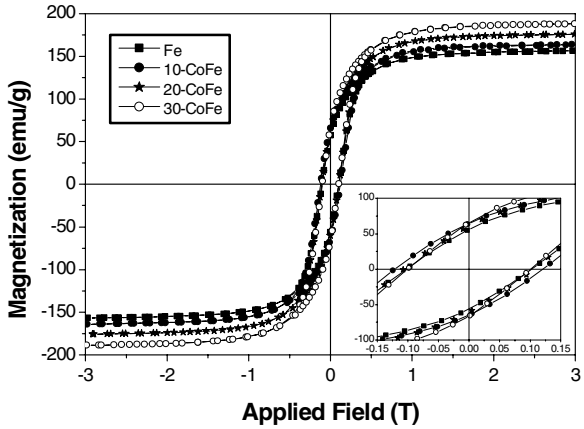

Figure 13. Hysteresis loops for the metal particles at room temperature.

3.4. Magnetic properties of the metal particles

Measurements of the magnetic properties, including hysteresis loops and time dependence of the magnetization variation at room temperature, were recorded as described in the experimental section. Figure 13 shows the hysteresis loops for the metal samples and the resulting hysteretic parameters are included in table 1. A linear dependence of the saturation magnetization on the cobalt content was observed. It should be noted that a small contribution to the saturation magnetization is to be expected from the different oxide content in each metallic particle. It is well known that the M_{s} values of bulk Fe (220 emu g^{-1}) can be increased by incorporating into the system small quantities of cobalt, where the highest magnetic moment is obtained for a Co content of 30 mol% (240 emu g^{-1}), according to the Slater–Pauling curve [27]. In accord, sample 30-CoFe presents the maximum value of saturation magnetization (180 emu g^{-1}). This value is among the highest reported value for metal particles of similar size [12, 25, 26, 28] (table 1).

On the other hand, a clear increase in the coercivity is observed for the sample with 10% of Co (1200 to 1075 Oe in pure iron). The needle-like nanoparticles have high shape anisotropy and in this case there is a proportional relationship between the coercivity and the saturation magnetization [1]. Therefore, the increment of the saturation magnetization in

Table 1. Morphological characteristics (TEM), crystal size (XRD), oxide content (Mössbauer) and magnetic properties at room temperature of FeCo nanoneedle particles (M_s = saturation magnetization, H_c = coercive field, V_{act} = activation volume).

	Particle size (TEM)				Magnetic properties		
Metal sample	Length (nm)	Width (nm)	Oxide content (Mössbauer) (%)	Crystal size (XRD) (nm)	M_s (emu g^{-1})	H_c (Oe)	V_{act} (10^{-17} cm^3)
Fe	210 (20)	45 (5)	38	32	145	1075	0.82
10-CoFe	200 (20)	40 (5)	18	26	158	1200	1.12
20-CoFe	215 (15)	44 (4)	20	21	170	1060	0.77
30-CoFe	250 (30)	50 (7)	23	18	180	1005	1.04

the nanoneedles produced by this compositional modification could yield an enhancement of the coercivity. However, the inverse tendency is found for samples with higher Co contents (20-CoFe and 30-CoFe). This effect could be a result of the competing contributions of the shape and crystalline anisotropies. As we discuss above, the contribution of the shape anisotropy increases with the value of M_s whereas the magnetocrystalline anisotropy constant, K_1, could decrease in this process, as has been observed in FeCo BCC bulk systems [29]. So, the evolution of the effective magnetic anisotropy with the Co content gives rise to the observed dependence of the nanoneedle coercivity. On the other hand, the heterogeneous Co distribution and the porosity present in the last two samples may also influence the reversal magnetization mechanism.

The viscous change of the magnetization after saturation and further application of a negative field of 800 Oe is shown in figure 14. The decays show the expected linear dependence of the magnetization on the logarithm of time [30], which allows us to calculate the magnetic viscosity coefficient S and the switching or activation volume [19]. The activation volume is expected to be close to the physical size in particles where reversal is similar to coherent rotation, and to be lower when the reversal is incoherent or heterogeneous. It can be seen that the activation volume of reversal for all these samples is clearly smaller than the physical volume of the particles as determined by TEM (table 1). Switching volumes similar to the physical size have only been found in iron oxide particles with a good structural order, whereas particles with shape and structure irregularities, or particles modified by addition of doping ions, present a smaller activation volume because of the lack of order, which makes more probable the occurrence of an incoherent or heterogeneous reversal [31, 32].

By comparing the physical particle volume calculated by TEM (about 14–18 $\times$ 10^{-17} cm^3) and the activation volume (between 0.8 and 1 $\times$ 1 $\times$ 10^{-17} cm^3), an average of 14–20 sub-units in each particle is obtained. Taking into account the crystal data obtained by x-ray diffraction, thermal activation seems to be related to the size of the crystallographic sub-units within the particle more than to the particle volume, in agreement with previous works [33]. Therefore, these nanoparticles can be described as composed by sub-units as observed by TEM, which is expected to give rise to an incoherent switching mode.

4. Conclusions

Uniform needle-like iron metal nanoparticles with Co contents up to 10% evenly distributed inside the particle have been obtained by coating haematite particles and their subsequent hydrogen reduction passing through the magnetite phase. Higher Co contents up to 30% were incorporated by coating the 10% Co-doped magnetite which produces a transition phase at the surface of the particles with decreasing amount of Co into the core. The microstructure of the metal particles seems to be composed by sub-crystals with the same crystallographic orientation inside the particle, their number depending on the Co content. On the other hand, magnetic characterization of the metal particles shows the highest reported saturation magnetization values for samples of similar size (180 emu g^{-1}) and coercivity values suitable to hard magnetic applications. We found that the highest value of coercivity (1200 Oe) was obtained for the sample containing 10% of cobalt, and the coercivity of the samples with higher cobalt quantity decreases as a consequence of internal microstructure changes and the competition of the shape and crystalline anisotropies.

Time dependence magnetization measurements showed that thermal activation is related to the size of the crystallographic sub-units within the particle rather than to the particle volume. The fact that the particles are composed of these sub-units gives rise to an incoherent switching mode.

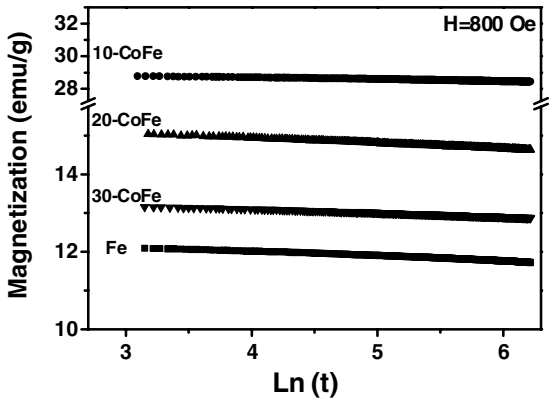

Figure 14. Time dependence variation of the magnetization at room temperature and constant magnetic field (800 Oe) for the different metal samples.

Acknowledgments

This work was supported by the CICYT under projects MAT2003-01479 and MAT2002-04001-C02 and the 'Acciones Integradas' project HF20020123. The fellowships of RP from the Spanish Ministerio de Ciencia y Tecnología and RMR from the Mexican CONACYT are gratefully acknowledged.

References

[1] Cullity B D 1972 *Introduction to Magnetic Materials* (Reading, MA: Addison-Wesley)
[2] Sharrock M P 2000 *IEEE Trans. Magn.* **36** 2420
[3] Sugimoto T 2000 *Fine Particles: Synthesis, Characterisation and Mechanism of Growth* (New York: Dekker) chapter 13
[4] Hisano S and Saito K 1998 *J. Magn. Magn. Mater.* **190** 371
[5] Bauer L A, Birenhaum N S and Meyer G J 2004 *J. Mater. Res.* **14** 517
[6] Hultgren A, Tanase M, Chen C S, Meyer G J and Reich D H 2003 *J. Appl. Phys.* **93** 7554
[7] Goia D V 2004 *J. Mater. Chem.* **14** 451
[8] Nuñez N O, Pozas R, Morales M P, Tartaj P, Bonville P, González-Elipe A R, Caballero A, Ocaña M and Serna C J 2003 *Chem. Mater.* **15** 951
[9] Pozas R, Ocaña M, Morales M P, Tartaj P, Nuñez N O and Serna C J 2004 *Nanotechnology* **15** S190
[10] González J M, Palomares F J, Hernando-Mañeru A, Morales M P, Serna C J and Cebollada F 2004 *J. Magn. Magn. Mater.* **272** 1528
[11] Nuñez N O, Tartaj P, Morales M P, Bonville P and Serna C J 2004 *Chem. Mater.* **16** 3119
[12] Ishikawa T and Matijevic E 1988 *Langmuir* **4** 26
[13] Matijevic E 1993 *Chem. Mater.* **5** 412
[14] Ocaña M, Morales M P and Serna C J 1999 *J. Colloid Interface Sci.* **212** 317
[15] Ozaki M, Kratohvil S and Matijević E 1984 *J. Colloid Interface Sci.* **102** 146
[16] Mendoza-Reséndez R, Morales M P and Serna C J 2003 *Mater. Sci. Eng.* C **23** 1139
[17] Mendoza-Reséndez R, Bomati-Miguel O, Morales M P, Bonville P and Serna C J 2004 *Nanotechnology* **15** S254
[18] Klug H P and Alexander I E 1974 *X-ray Diffraction Procedures* (New York: Wiley)
[19] Gaunt P 1986 *J. Appl. Phys.* **59** 4129
[20] Gillot B and Rousset A 1986 *J. Solid State Chem.* **65** 322
[21] Gillot B, Jemmali F and Rousset A 1983 *J. Solid State Chem.* **50** 138
[22] West A R 1984 *Solid State Chemistry and its Applications* (Chichester: Wiley) chapter 2
[23] Eiling A 1987 *IEEE Trans. Magn.* **23** 16
[24] Lee M S, Kim T Y, Lee C S, Park J C, Kim Y I and Kim D 2004 *J. Magn. Magn. Mater.* **268** 62
[25] Varanda L C, Jafelicci M, Tartaj P, O'Grady K, Gonzalez-Carreño T, Morales M P, Muñoz T and Serna C J 2002 *J. Appl. Phys.* **92** 2079
[26] Morales M P, Serna C J, O'Grady K, Prichard L S, Hutchings J A, Milford G H and Dickson D P E 1999 *J. Magn. Magn. Mater.* **193** 314
[27] Chikazumi S 1964 *Physics of Magnetism* (New York: Wiley) p 72
[28] Kishimoto M, Nakazumi T, Otani N and Sueyoshi T 1991 *IEEE Trans. Magn.* **27** 4645
[29] Wijn H P J 1991 *Magnetic Properties of Metals* (Berlin: Springer) p 37
[30] Aharoni A 1992 *Phys. Rev.* B **46** 5434
[31] Botoni G 1993 *J. Magn. Magn. Mater.* **3** 120
[32] Botoni G 1999 *J. Magn. Magn. Mater.* **196/197** 602
[33] Veitch R J, Richter H J, Poganiuch P, Jakusch H and Schwab E 1994 *IEEE Trans. Magn.* **30** 4074